IOP Publishing Journal Title
Journal **XX** (XXXX) XXXXXX https://doi.org/XXXX/XXXX

Energetic particle loss under the effects of the radial electric field in LHD

Ethan Green[1], Wataru Hayashi[1], Xishuo Wei[1], Zhihong Lin[1], Hiroyuki Yamaguchi[2], Masaki Osakabe[2,3], Hideo Nuga[2], Kunihiro Ogawa[2,3], Ryosuke Seki[2], Mitsutaka Isobe[2,3,4], Yasuko Kawamoto[2,3], Akihiro Shimizu[2,3], Takeshi Ido[5], and Masaki Nishiura[2,6]

[1] Department of Physics and Astronomy, University of California, Irvine, CA 92697-4574, United States of America
[2] National Institute of Fusion Science, National Institute of Natural Sciences, Toki 509-5295, Japan
[3] Graduate University for Advanced Studies, Toki, Gifu 509-5292, Japan
[4] Mahasarakham University, Chang Wat Maha Sarakham 44150, Thailand
[5] Kyushu University, Kasuga, Fukuoka 816-8580, Japan
[6] The University of Tokyo, Kashiwa, Chiba 277-0882

E-mail: ethanmg@uci.edu

Received xxxxxx
Accepted for publication xxxxxx
Published xxxxxx

Abstract

The impact of the radial electric field (E_r) on the confinement of energetic particles in the Large Helical Device is studied through gyrokinetic simulation. Particle orbits are characterized as passing, helically trapped, and barely trapped. E_r has little effect on passing particles. A positive E_r is found to improve the confinement properties of trapped particles by increasing their precession rate, thereby reducing radial drift over a bounce motion. A negative E_r is found to do the opposite. E_r can induce particles to change orbit topology. The effects of an experimental E_r profile are discussed. Overall, positive E_r is found to improve while negative E_r is found to degrade confinement of energetic particles. Furthermore, the lost energetic particles originate from localized regions of phase space. Knowledge of which can be utilized to induce radial current to control E_r by injecting neutral beams into these regions.

Keywords: stellarator, radial electric field, energetic particle

1. Introduction

Stellarators rely on complex three-dimensional (3D) magnetic fields to confine plasma, offering both advantages and disadvantages compared to tokamaks [1], [2]. The main advantage of stellarators is that they do not require an induced current to maintain the magnetic field structure required to confine the plasma. This nearly eliminates the entire class of instabilities known as current driven instabilities from consideration in stellarators. Furthermore, to induce this current in a tokamak, we continuously ramp up the current through a part of the machine called the central solenoid. As we can not increase current forever, tokamkas must either use other methods to produce a toroidal current or periodically reset, which can damage the machine. Since this current ramp up is not required in a stellarator, stellarators are inherently closer to steady state devices. The main advantage of tokamaks is their axisymmetric magnetic field configuration, which reduces the equilibrium geometry of confinement to two dimensions, ensuring that collisionless particle orbits are

confined to closed paths. This symmetry is a key reason energetic particles (EPs), such as fusion-born alpha particles, are well confined in tokamaks in the absence of collective instabilities such as Alfven eigenmodes. In stellarators, however, the lack of exact axisymmetry results in the loss of EPs, posing a challenge for their confinement. For a fusion device to operate effectively, alpha particles must transfer their energy to the thermal plasma before escaping confinement, thereby providing the necessary heating to sustain further fusion reactions. Therefore, the confinement of EPs is a fundamental problem that must be addressed in stellarators [3], [4], [5], [6].

The EP and thermal plasma confinement can be affected by radial electric field (E_r), $E_r = \vec{E} \cdot \hat{e}_r$ where $\hat{e}_r$ is the radial unit vector pointing out of the magnetic axis. In tokamaks, E_r shear is known to create transport barriers that suppress turbulence and reduce radial transport of particles and heat [7], [8]. Similarly, in stellarators, both E_r and E_r shear can influence the transport of thermal plasma and energetic particles [9], [10], [11], [12], [13], [14], [15], [16]. E_r may also be used to expel impurities from the core [10], [11]. Experiments on the LHD have further demonstrated that E_r can significantly impact plasma profiles [17] and that a positive E_r can improve confinement [18], [19]. Gyrokinetic simulations of Wendelstein 7-X (W7-X) have shown that E_r in the electron root can suppress microturbulence [20]. These findings motivate a deeper exploration of the role of E_r in stellarator confinement.

Because of their high energy, EPs rarely undergo collisions, meaning that their motion is mostly free streaming [21] and can be well understood based on collisionless, gyrokinetic simulations. Optimization of stellarators for improved EP confinement is a central problem in stellarator research[22]. This work will contribute to future studies on using E_r and potentially varying E_r to further such optimizations.

The equilibrium E_r arises from non-ambipolar (unequal) fluxes of ions and electrons within the stellarator plasma, with its characteristics depending on the ion and electron temperatures and neoclassical transport. It has been shown that in LHD, neoclassical transport plays a significant role in the generation of this non-ambipolarity [23]. There are two potential regimes for E_r, the ion root and electron root. In the electron root, high electron temperatures allows trapped electrons to diffuse outwards radially faster than ions, resulting in a positive electric field. Conversely, in the ion root, higher ion temperatures lead to faster ion diffusion and a negative radial electric field[12]. E_r is the component of the Electric field that points radially outwards from the magnetic axis, so a positive E_r means that $\vec{E}$ points outwards from the magnetic axis while a negative E_r means that $\vec{E}$ points radially inwards, towards the magnetic axis. These ambipolar electric fields can affect the EP confinement.

EPs in turn can affect E_r as well as thermal confinement. Both effects have been studied in tokamaks [22], [23]. As shown in [17], E_r can be changed by varying the perpendiciular neutral beam injection power, but is mostly unaffected by varying the parallel injection power. This implies that to analyze the effects of EP on E_r, we need a better understanding of how E_r affects EPs at different locations in phase space.

To obtain such an understanding, we have carried out two experiments on LHD to measure the effects of particle injection at different pitch angles $\lambda = B_0\mu/\mathrm{E}$ where B_0 is the magnetic field strength on the magnetic axis, μ is the magnetic moment and E is the kinetic energy of a particle. In the first, we found that we needed a higher plasma density to reduce the effects of charge exchange losses. Nonetheless, we obtained an electron root E_r profile from this experiment, which is discussed in this paper. The second experiment will be discussed in a future paper analyzing the effects of varying NBI energy and pitch angle on E_r.

The main difference between trapped particles in LHD (or any heliotron) and a tokamak is that trapped particles in LHD precess through a helical magnetic field well and thus precess poloidally as well as toroidally. In an electrostatic simulation with radial electric field, only curvature and grad-B drift contribute to the radial motion of particles. As B is a function of position, decreasing the rate of helical precession increases time spent drifting in one direction radially, increasing radial excursion over a transit through the helical B field well.

We show through gyrokinetic simulation that a positive E_r improves the confinement of trapped particles, while a negative E_r degrades the confinement of trapped energetic particles in the LHD. This is fairly surprising, as one would expect that a positive E_r would eventually push ions radially outwards. Negative E_r decreases the helical precession rate of trapped particles,

increasing radial excursion and allowing some trapped particles to reach the separatrix and others to transition to barely trapped orbits. As barely trapped particles do not conserve the second adiabatic invariant $J_{||}$ these particles are often able to leave the plasma increasing EP losses due to negative E_r. Positive E_r does the opposite. By increasing helical precession, positive E_r reduces radial excursion of trapped particles, reducing both the number of trapped particles that reach the separatrix and the number of trapped particles that reach a region of low enough magnetic variation that they change to a barely trapped orbit. We further analyze how the electric field measured in experiments on LHD affects the particle distribution, focussing on particles at different positions in phase space. Another surprising result is that a small E_r, sourced by potential variation across the radial domain on the order of 5 kV can have a significant effect on the loss of EPs at all energies tested, up to at least 60 keV, although it does have a greater effect on particles in the lower energy range. Finally, the lost particles originate from localized phase space regions, which can be utilized to control Er by injecting neutral beam into these regions to induce radial current. This analysis will need to be carried out in a future fusion reactor for particles with energies ranging up to the expected α particle birth energy of 3.5 MeV.

This paper is organized as follows: Section 2 details the simulation parameters and codes used in this study. Section 3 examines particle orbits in LHD and the effects of imposed, constant E_r profiles. Section 4 presents an analysis of simulations with experimentally informed E_r profiles. Finally, Section 5 summarizes the results and discusses their implications.

2. LHD Experiment and Simulation

The parameters of the simulations discussed in this paper are taken from shot #183281 of the LHD [26]. This shot was taken from an experiment attempting to find the dependance of E_r on the pitch angle of injected particles, and was chosen for its magnetohydrodynamic quiescence and E_r data. This shot was taken in the standard configuration, where the magnetic field on axis is $B_0 = 2.64\,T$ and the major radius is $R_0 = 3.75\,m$. Electron cyclotron heating is used to increase the electron temperature, enforcing an electron root E_r. Energetic particles are sourced by neutral beams (NBI) 3 and 4, providing a counter passing and trapped EP population respectively, although we leave the study of the effects of realistic NBI profiles on E_r to a later paper. Due to the helical field coils, the magnetic field in LHD always has right handed helicity. The toroidal magnetic field points clockwise when viewed from above. This allows use of the Heavy Ion Beam Probe (HIBP) to measure electrostatic potential in the core[27], [28]. For each time slice, the HIBP provides the electrostatic potential (in kV) at various values of the effective radius, which is the radius of a simple torus with the same enclosed volume as the flux surface of interest [29].

This paper focusses on simulations of this shot using the Gyrokinetic Toroidal Code (GTC) [8]. The simulations need the equilibrium state that the plasma maintains within an imposed magnetic geometry. In this study, we use the Variational Moments Equilibrium Code (VMEC) [30] to generate this equilibrium. Specifically, it is used to solve for the equilibrium magnetic field and plasma currents within LHD. These quantities are transformed to the Boozer coordinates including poloidal flux function ψ, poloidal angle θ, and toroidal angle ζ using BOOZ_XFORM [31]. The B field in these coordinates is pointed in the $+\theta, +\zeta$ direction. Throughout this paper, the radial coordinate will be normalized by ψ_w, the poloidal flux function at the separatrix.

Two types of E_r profiles are imposed on the simulation as equilibrium data. In Section 3, we discuss the simpler case of simulations with an E_r of 0 or ± 5 kV/m imposed over the entire domain to understand the effects of E_r on orbit topology and particle loss. The magnitude of E_r in shot #183281 is slightly larger than these values through most of the radial domain, so $\pm$5kV/m was chosen to provide a conservative estimate of the effects of E_r. In Section 4, we assess the effects of realistic E_r using experimentally measured E_r profiles. While GTC is capable of running self-consistent electromagnetic simulations [32], in this work, we allow neither the magnetic fields nor E_r to change in time. So in our simulations we are pushing guiding centers according to the background magnetic field and imposed E_r. The slowing down time for EPs under the experimental conditions is ~0.15s, many orders of magnitude beyond the simulation time we are examining, so we exclude collisions as well to focus on collisionless losses.

In our simulations, we use a uniform distribution of deuterium particles with kinetic energies ranging from 20 to 60 keV. This energy range is chosen to match the

energies of particles deposited by the perpendicular neutral beam as these are the EP's that are experimentally accessible and most affected by E_r. A substantial fraction of these particles near the separatrix are lost within one transit or bounce time, regardless of E_r. We consider a particle to be lost when it passes the last closed flux surface (LCFS). This likely leads to overestimates of particle losses[19]. Note that we use the terms LCFS, ψ_w and separatrix interchangeably in this paper. To remove these first-orbit losses, we perform an initial simulation without E_r for a tranist time τ_o= 16 μs, to identify and exclude the lost particles, and then rerun the simulation from the beginning with the defined E_r profiles. Here τ_o is calculated as $\tau_o = 2\pi R_o/\sqrt{2T/m_i}$. T=20 keV is the minimum energy EP used in this simulation and m_i is the mass of deuterium. This approach allows us to isolate and better visualize the effects of E_r on particles that remain confined in the plasma core over longer timescales.

3. Effects of Constant E_r on Orbit Topologies

In stellarators, there are three primary orbit topoplogies [5], [33]. These are labeled here as passing, trapped and barely trapped. Within LHD and other heliotrons, trapped particles precess helically around the magnetic axis, so we label them as helically trapped. These three particle orbits are defined as follows:

- Passing: Particles that move predominantly parallel or antiparallel to $\vec{B}$ and do not reverse direction with respect to $\vec{B}$.
- Helically Trapped: Particles confined between the helical magnetic field maxima, forming mirror-like orbits in the region of minimum |B|.
- Barely Trapped: Particles that alternate between passing and helically trapped states. Barely trapped particles are passing or counter-passing on the outer side of the torus, often completing multiple toroidal transits before reaching the inner side of the torus, where they may bounce back [4].

Additionally, there are ripple-trapped particles, which become trapped in small magnetic field wells caused by field perturbations or imperfections which are not included in this simulated equilibrium. In section 3.3, we further classify barely trapped particles into two subcategories: helical boundary orbits and banana-like orbits.

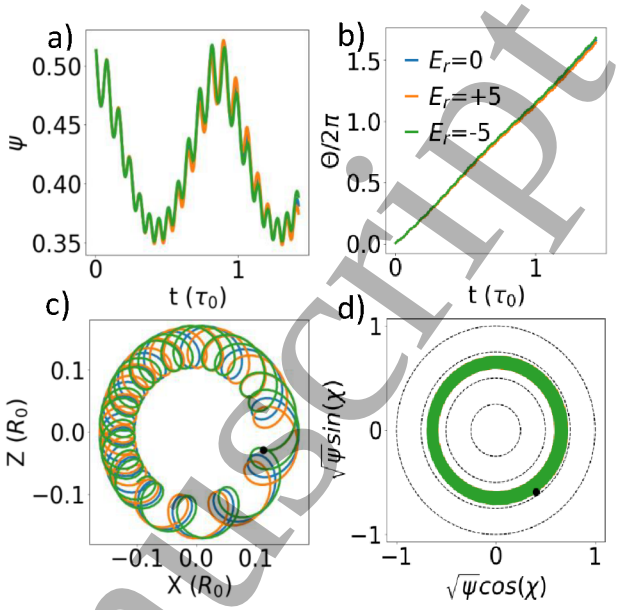

Figure 1 Trajectories of a co-passing particle with initial $\lambda = 0.11$ and kinetic energy E = 59825 keV under different radial electric fields, E_r values in kV/m a) ψ as a function of time. b) Poloidal angle θ as a function of time. c) Projection of particle trajectory in real space on the plane moving toroidally with the particle d) Particle trajectory on plane rotating with the minimum B field. The starting point of the particle in c and d is marked with a black dot

3.1 Passing particles

Passing particles are characterized by a low pitch angle λ. Thus co-passing particles, those that move mostly parallel to the magnetic field, are most simply characterized by $v_{||}/v \approx 1$ where $v_{||} = \vec{v} \cdot \hat{b}$ and $\hat{b}$ is the unit vector in the direction of $\vec{B}$, while counter-passing particles, those that move mostly antiparrallel to the magnetic field, are most simply characterized by $v_{||}/v \approx -1$. A passing particle orbit is illustrated in Figure 1. As these particles move towards the inner side of the torus, they drift slightly toward the magnetic axis. Conversely, when they travel towards the outer side of the torus, they drift away from the magnetic axis. Opposite to co-passing particles, counter-passing particles drift towards the axis as they approach the outside and away from the axis as they approach the inside of the torus. These particles are well confined as their radial drift cancels itself out over a poloidal transit.

As shown in Figure 1 the guiding center orbits of passing particles remain largely unaffected by the presence of E_r. In this equilibrium, the $E \times B$ velocity due to a positive E_r slightly shifts the poloidal angular velocity of a passing particle orbit towards the negative θ-direction, while a negative E_r shifts it in the positive θ-direction for passing particles. Figure 1b shows the poloidal position of the particle as a function of time. Note that the outer side of the torus is at $\theta = 2\pi n$ in our simulation for an integer n. We allow θ to go beyond 2π in this and future plots to more directly show when a particle changes direction poloidally. Figure 1c shows the projection of the particle's orbit on a plane moving with the particle toroidally. $X = R/R_0 - 1$ where R is the major radius and R_0 is the major radius at the magnetic axis. The small loops in Figure 1c come from the topology of the magnetic field line that the particle follows. The circular shape traced by all of these smaller loops can be viewed as a toroidal average of the flux surface shape. Figure 1d shows the particle's orbit projected onto a plane rotating with the magnetic field strength. $\chi = 2\,\theta - 10\,\zeta$ is the helical direction in LHD, which has a dominant helical B(m =2,n=10) field. The m and n are the poloidal and torodal mode numbers.

3.2 Helically trapped particles

Helically trapped particles are the dominant type of mirror-trapped particles in the LHD. They bounce within the local low-|B| field well of the stellarator's magnetic configuration [5]. In this paper, we refer to them as helically trapped particles because, in LHD, the dominant magnetic field variation is B(2,10). Accordingly, the magnetic field well rotates helically around the magnetic axis.

Helically trapped particles have high λ and exist in regions of low |B| on a flux surface. Their trajectories form small banana-shaped orbits as they drift helically. As with all trapped particles, under no E_r, the bounce points occur at the same value of |B| to conserve both μ

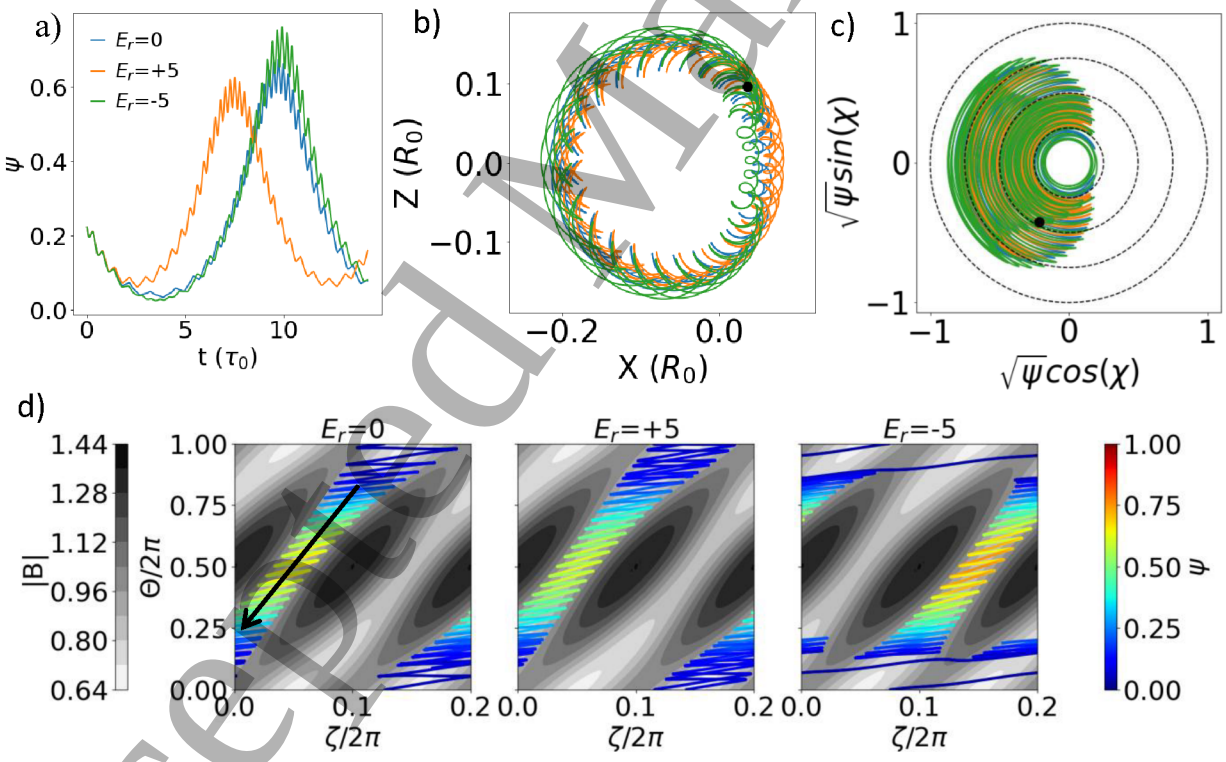

Figure 2 Trajectories of a helically trapped particle with $\lambda = 1.03$ and E = 44636 keV under different radial electric fields. E_r values in kV/m. a) ψ as a function of time. b) Projection of particle trajectory in real space onto constant poloidal plane. c) Particle trajectory on plane rotating with the minimum field d) Particle orbit on ζ, θ plane over contours of magnetic field strength at $\psi = 0.5$ normalized to B_{ax}. Trajectory color in panel d represents radial coordinate. The arrow shows the direction of precession

and E. Under an E_r, the radial drift will change the potential energy of the particle, and thus the kinetic energy and bounce point must shift to compensate. These particles exhibit radial drift: they drift outward as they precess toward the inside of the torus and inward as they move toward the outside of the torus, as shown in Figure 2d. These particles precess in the $-\theta, -\zeta$ direction within the field well, along the helical contour defined by χ = constant [3]. It follows that, helically trapped particles are predominantly lost on the inner side of LHD when their radial drift moves them out toward the last closed flux surface (LCFS).

As shown in Figure 2, E_r significantly affects helically trapped particles. Radial drift comes from the radial component of ∇B and curvature drifts, which points inwards for $\theta < \pi$ and outwards for $\theta > \pi$. For a positive E_r, E x B drift points in the same direction as the component of ∇B and curvature drift that is tangential to a flux surface, thus increasing the rate of precession of a trapped particle through the helical B field well and decreasing the time the particle spend drifting radially in one direction. Consequently, positive E_r reduces the radial drift over a full toroidal transit through the magnetic field well. Conversely, a negative E_r results in E×B drift that counteracts the component of ∇B and curvature drift tangential to a flux surface, decreasing the rate of precession and thus increasing net radial drift [9]. Another way to view this effect is that increasing the rate of precession can help push trapped particles through the higher magnetic field strength on the inside of the torus, allowing the particle to pass through $\theta = \pi$ where it drifts towards the magnetic axis. Without this extra push, the particle may continue bouncing in a region where its net radial drift over any bounce motion is outwards until it exits the plasma. A particle that does exactly this is shown in figure 6.

In the case of the particle shown in Figure 2, a negative E_r significantly altered the particle's orbit topology as well. The increased radial drift allowed the particle to drift far enough inward to reach a flux surface where the magnetic field variation was small enough to prevent trapping. As a result, the particle temporarily transitions to a counter-passing orbit, making it, as we later define, a helical boundary orbit, completing some

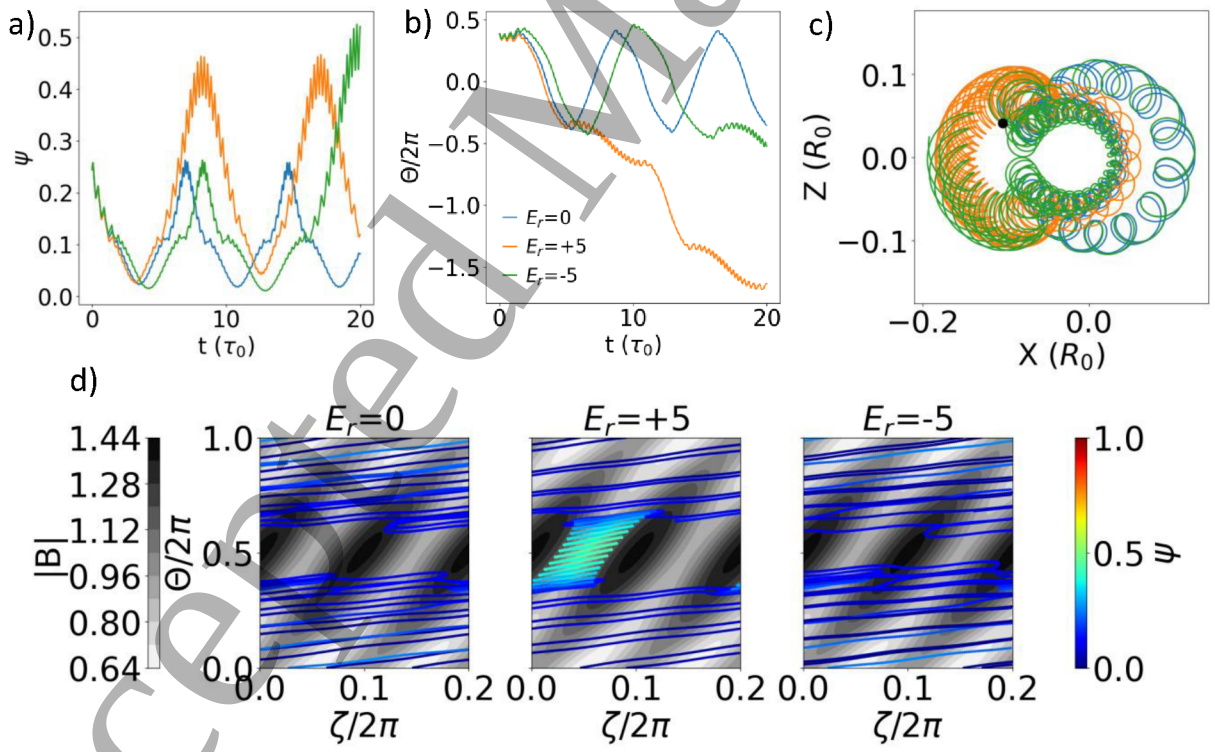

Figure 3 Trajectories of a barely trapped particle with $\lambda = 0.897$ and E = 59080 keV under three different E_r. a) ψ as a function of time. b) Poloidal angle θ as a function of time. c) Projection of particle orbit in real space onto constant poloidal plane. d) Particle orbit on ζ, θ plane over contours of magnetic field strength at $\psi = 0.3$ normalized to B_{ax}. Trajectory color in panel d represents radial coordinate. Er values in kV/m

poloidal transits before drifting outward and reentering a trapped orbit. These poloidal transits are visible in figure 2b, where we see loops in the green line on the right side of the figure as well as in figure 2c, when the particle crosses the line $\chi = 0$, making circles near the axis. It then drifts farther outward than its counterparts in the $E_r = 0$ and $E_r = +5$ kV/m cases. This demonstrates that E_r can influence not only particle motion within a given orbit topology but also induce transitions between different orbit topologies. However, this effect is likely inflated in this simulation due to the unphysical nature of a constant E_r near the magnetic axis.

3.3 Barely trapped particles

Barely trapped orbits have intermediate values of λ—lower than those of helically trapped particles but higher than those of passing particles. These particles are typically in a passing or counter-passing state on the outside of the torus but can become trapped on the inside of the torus, particularly at larger radial positions where the magnetic field variation is more pronounced. Figure 3 shows a particle in a barely trapped orbit. Barely trapped particles generally have complex trajectories and do not necessarily return to the same bounce point. Consequently, their radial drift does not vanish when averaged over a bounce motion [8], leading to the poor confinement properties shown in Figure 8 for particles of λ values ~0.8.

In heliotron configurations, barely trapped orbits can be categorized into two distinct types: banana-like orbits and helical boundary orbits. The key distinction lies in the behavior of these particles on the inside of the torus. Helical boundary particles can traverse the inside of the torus on a helically trapped orbits, whereas banana-like particles cannot as they are reflected back to the outside of the torus by the larger |B| field on the inside. In other words, banana-like particles are trapped by the secondary magnetic field variation of LHD, B(1,0) due to toroidicity, like banana orbits in tokamaks. However, their trajectories are poorly confined due to the lack of axisymmetry.

Barely trapped particles often complete several toroidal transits on the outside of the torus in a passing or counter-passing state. As they drift toward the inside, their parallel motion is suppressed by the increasing B(1,0) field strength. On the inside, they may exhibit small helically trapped bounces.

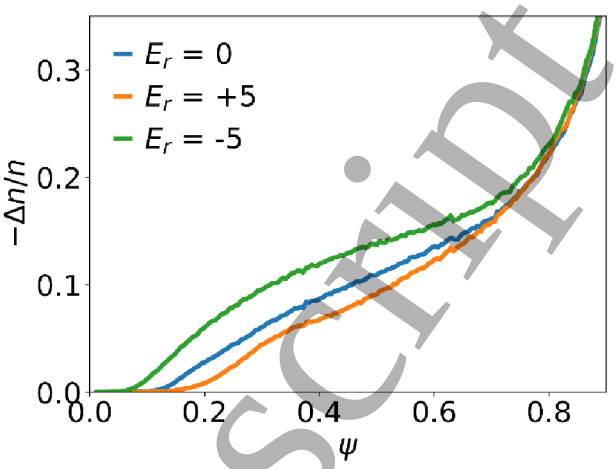

Figure 4 Loss fraction as a function of initial radial location ψ showing lost particles from simulations with constant E_r of +5, 0, -5 kV/m. Initial distribution is isotropic. First orbit losses are not shown

The particle in Figure 3 in the simulation with E_r=0 kV/m is in a banana-like orbit. Banana-like particles reverse the direction of their poloidal motion upon reaching the larger magnetic field on the inside of the torus. They do not cross the maximum poloidal |B| value. The simplest way to identify banana-like particles is that they do not pass through the inside of the torus, $\theta = \pi + 2\pi n$ in our simulations. Banana-like particles occasionally make a few regular banana type bounces on the inner side before reversing directions along the χ=constant contour.

Helical boundary particles behave similarly to banana-like particles but can pass through the inside of the torus by making helically trapped bounce motions on that side. In LHD, helically trapped particles generally precess in the $-\theta, -\zeta$ direction as designated by the arrow in figure 2d. Helical boundary particles maintain this directionality when in a helically trapped or counter-passing state. However, some can briefly reverse helical precession direction while they drift outwards, allowing them to drift in a small loop. This type of motion, referred to as "periodic banana drift convection" [5] or classically as a "superbanana" [3], [34], is fairly uncommon in LHD. In figure 3, the particle in the simulation with E_r=+5 kV/m is in a helical boundary orbit.

While helical boundary and banana-like orbits have distinct properties, particles frequently transition between these two orbit types during their motion. For example, the particle shown in Figure 3 initially begins

on a trapped orbit before quickly tranitioning to a counter passing orbit. In the simulation with E_r=-5kV/m, the particle makes two bounce motions on a banana like orbit before transitioning to a helically trapped orbit at ~$15\tau_0$ where it then drifts further out radially. These transitions between trapped and passing state constitutes a breaking of the secondary adiabatic invariant $J_{||}$, providing another reason barely trapped particles are poorly confined [35].

As is clear from examining figure 3, the presence of E_r can influence these transitions. In the positive E_r case, the particle is imediately pushed into a helical boundary orbit while in the negative E_r and no E_r cases, the particle quickly transitions to a banana-like orbit. The observations in this section demonstrate that E_r not only affects the radial drift and angular separation of barely trapped particles but also determines their transitions between different orbit topologies.

3.4 E_r effects on collisionless losses

Figure 4 shows the fraction of EPs lost as a function of their initial radial position in simulations with constant positive, negative, and no E_r. As shown simulations find that, a positive E_r improves the confinement of EPs, while a negative E_r degrades it. This is due to the poorer confinement of helically trapped and barely trapped particles in a negative radial electric field explained in sections 3.2 and 3.3. A scan of E_r up to magnitude 30kV/m was performed with larger magnitudes strengthening the effects described.

If an external E_r has a transition from positive to negative, the ratio of lost particles is bounded by the ratios observed in cases with constant E_r at the extremal values off the changing case. While the specific mechanisms by which a changing-sign E_r impacts the confinement properties of the particle distribution remain to be fully understood, we can conclude that both the sign and magnitude of the local E_r play an important role in collisionless EP loss.

3.5 Summary of effect of E_r

As demonstrated, the E_r can have various impacts on particle orbits in the LHD, depending on the orbit type as well as the sign and magnitude of E_r. The key results and logical conclusions relevant to the next sections are summarized below:

1. E_r has little to no long term effect on passing particles
2. Negative E_r decreases the rate of precession of helically trapped particles, and thus increasing radial excursion. This degrades confinement of helically trapped particles. Negative E_r can also cause some helically trapped particles to transition into barely trapped orbits which are even more poorly confined.
3. Positive E_r increases the rate of precession of helically trapped particles, reducing radial excursion. Due to the reduced radial excursion, helically trapped orbits are better confined in positive E_r. Positive E_r also pushes particles in barely trapped orbits towards better confined helically trapped orbits.

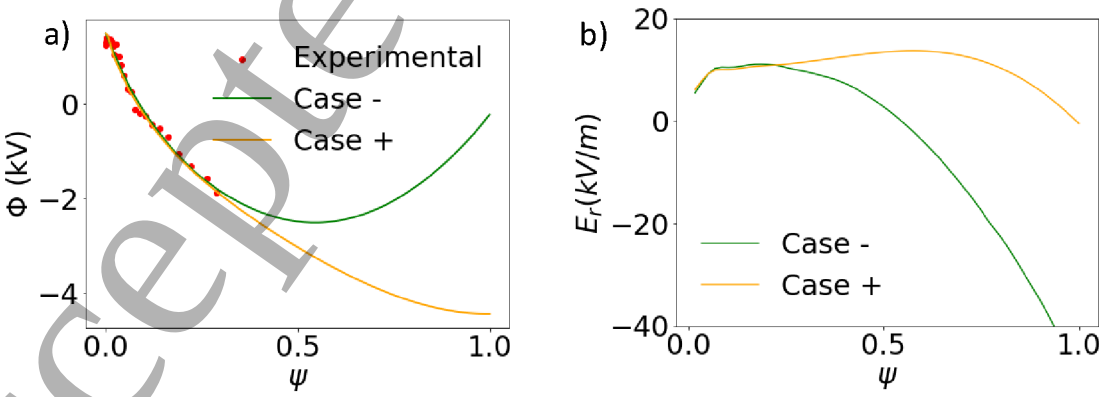

Figure 5 a) Potential data imposed on simulation based on HIBP data from shot #183281 in LHD at 4.2s. b) corresponding radial electric field. Case – potential data is extrapolated such that $\phi = 0$ at ψ_w while Case + is extrapolated such that $\nabla\phi = 0$ at ψ_w.

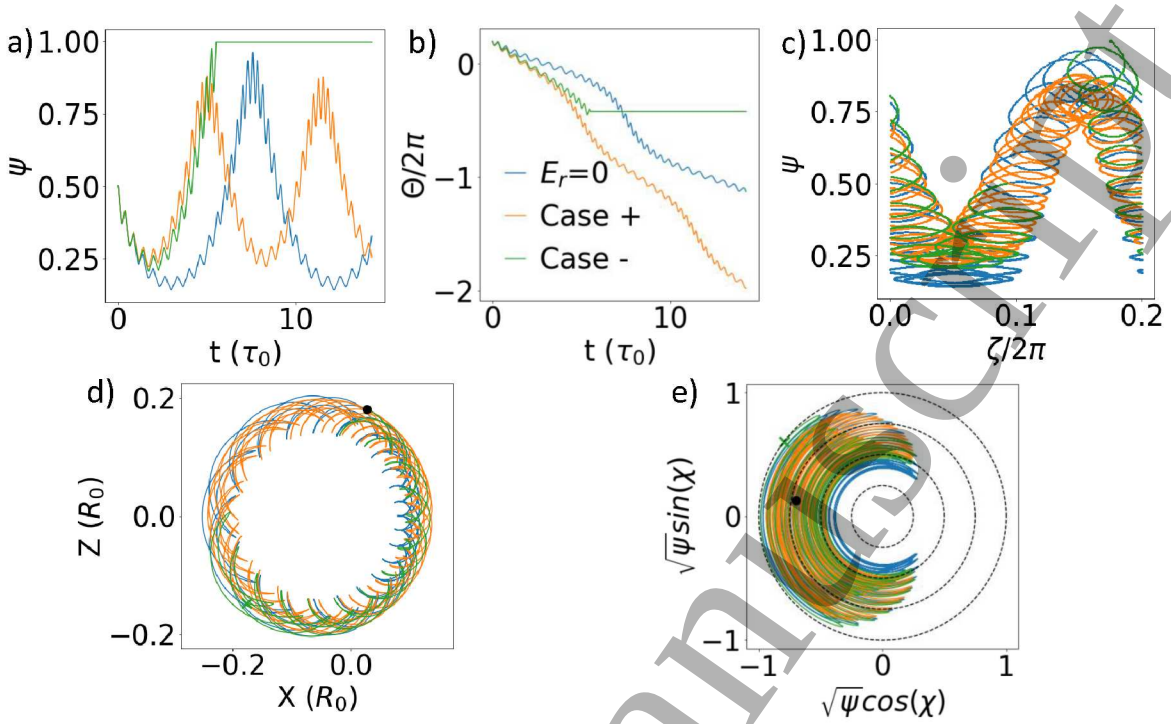

Figure 6 Trajectories of a helically trapped particle with $\lambda = 1.05$ and E = 40854 keV under experimental E_r a) ψ as a function of time. b) θ as a function of time. c) particle motion in ψ and ζ direction d) Projection of particle orbit in real space onto constant poloidal plane. e) Particle orbit on plane rotating with the minimum B field. In d and e, the point at which the particle in Case - is lost is marked with green x mark.

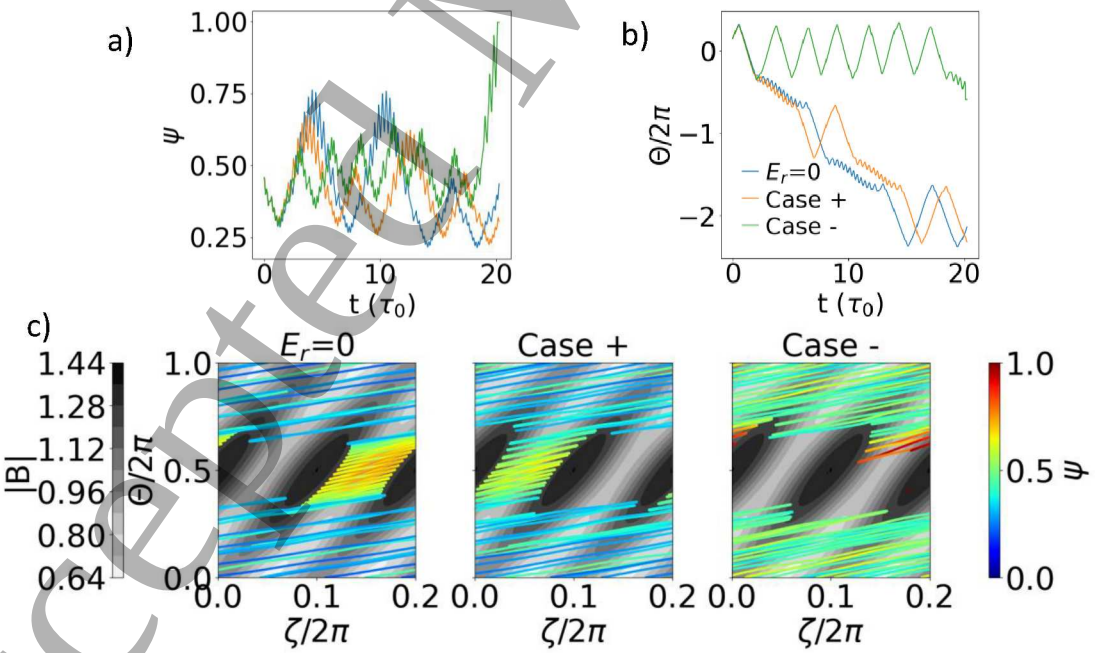

Figure 7 Trajectories of a barely trapped particle, $\lambda = 0.897$ E = 59 keV, under experimental E_r a) ψ as a function of time. b) Poloidal angle θ as a function of time. c) Particle orbit on ζ, θ plane over contours of magnetic field strength at $\psi = 0.5$ normalized to B_{ax}. Trajectory color in panel d represents radial coordinate.

4. Experimental E_r Profile

To study the effects of a realistic E_r profile on EP confinement, we use data collected 4.2 seconds into LHD shot #183281. The HIBP data extends to approximately $\psi \cong 0.3$. Since the data does not cover the entire plasma minor radius, we extrapolate it outward using two different boundary conditions to simulate up to the LCFS. The experimental data as well as the corresponding potential and E_r profiles are shown in Figure 5.

Case – For the first boundary condition, we require the potential to be zero at the ψ_w, producing a negative E_r beyond the experimental data region. This profile, labelled "Case –," results in poorer confinement properties. Note that the negative E_r strength near ψ_w of this case is stronger than experimentally observed E_r in similar shots. This does not change the qualitative arguments within this paper, as E_r on the order of -5kV/m as used in the previous section is a reasonable and conservative value near the separatrix. It will however lead to somewhat greater losses shown in figures 8, 9, and 10 than would be physical.

Case + For the second boundary condition, we extend the potential smoothly with a negative slope up to ψ_w, resulting in a positive E_r profile labeled "Case +" which improves confinement.

As shown in Figure 2 a and e, radial drift during a bounce motion is larger at higher ψ, where the magnetic field variation over a bounce is greater. This effect is further compounded when there is a strong negative E_r at the outer edge of the plasma, as in Case – slowing down trapped particle precession, giving them more time to drift radially. As the outer edge is closer to

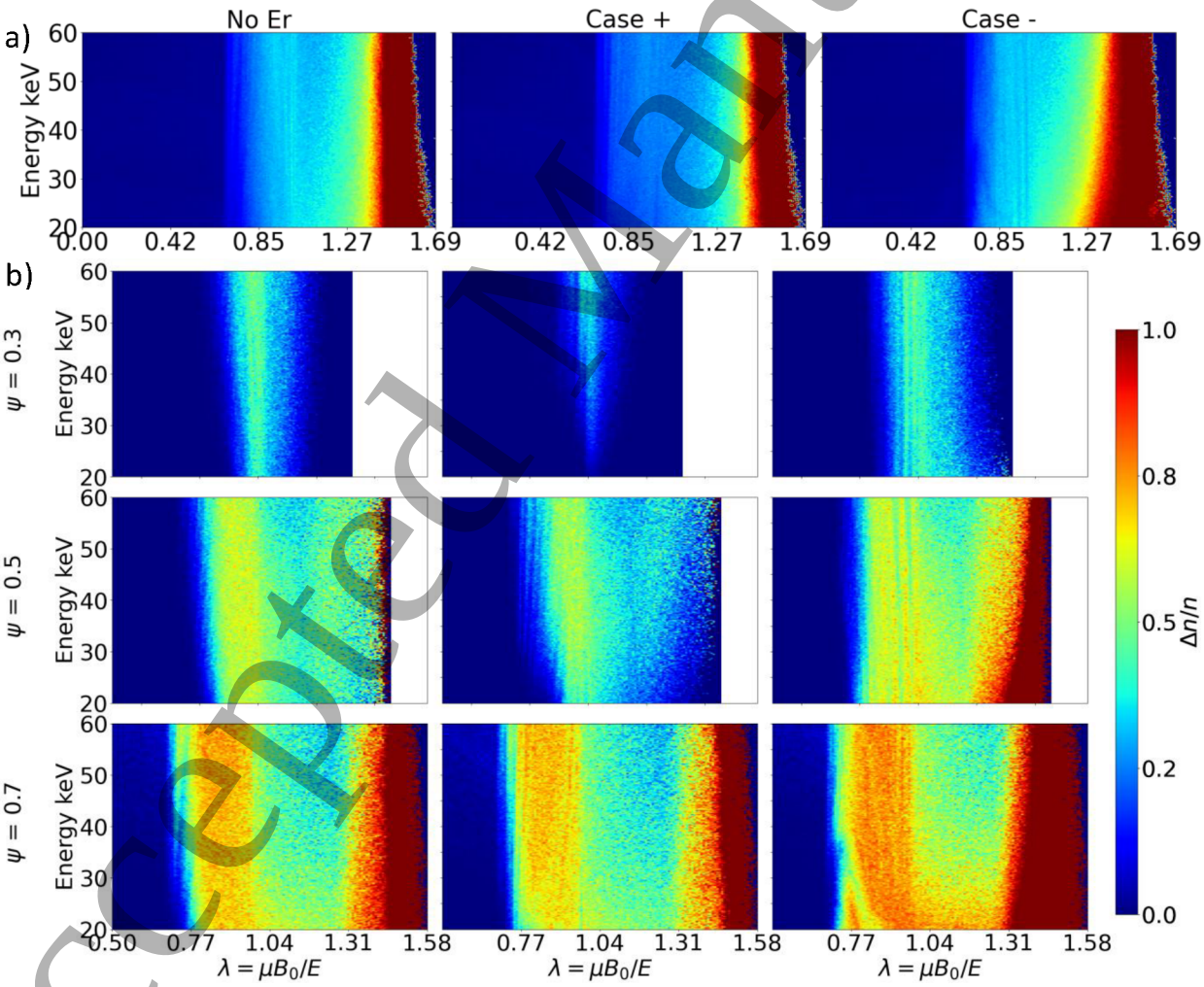

Figure 8 Fraction of particles lost as a function of their initial phase space coordinates a) full volume, b) particles initialized on specified flux surfaces

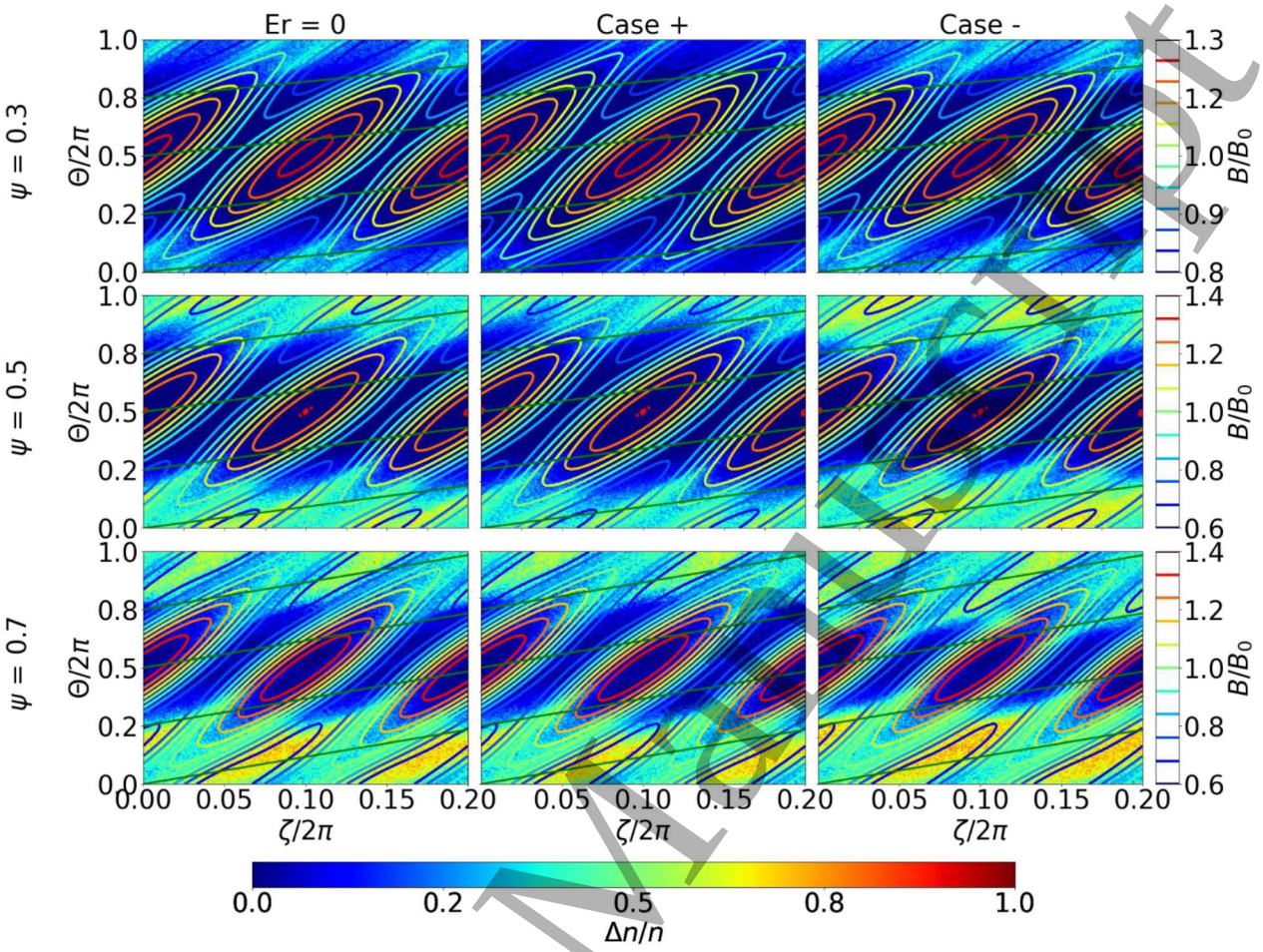

Figure 9 Lost particles' original position on different flux surfaces. First orbit losses are already removed. Contours show B field strength. Lines show magnetic field direction in the $+\theta, \zeta$ direction.

the separatrix this increases the likelihood of particle loss. Consequently, helically trapped particles in Case – are more likely to be lost compared to the No E_r case.

This effect is demonstrated clearly in Figure 6, which shows the motion of a helically trapped particle under the effects of the experimental E_r profiles. Under the E_r of Case -, the particle is lost at around 6 τ_0. As shown, under all 3 different cases of E_r, the particle remains in a helically trapped orbit. The positive E_r of Case + causes the banana orbits to tighten up, and drift less over poloidal transit as illustrated by the vertical width of the loops and total periodic motion in Figures 6a and 6c and the tightness of the banana (smaller angles at the tips and decreased area enclosed) in 6d. As shown in Figures 6 a,b,c the particle in Case – acts similarly to that in Case + until it drifts out further radially, ψ~0.6. Here it reaches a region of lower and then negative E_r, reducing the poloidal precession and significantly increasing the radial drift over a single bounce motion. This allows the particle to drift far enough to reach the separatrix, as shown in figure 6c.

Figure 8 shows the fraction of particles lost from their initial phase space positions. The negative E_r at the edge of Case – causes helically trapped particles with relatively high values of λ to be lost more readily. This is evident in Figure 8a, where the high-λ cutoff for lost particles shifts downward in Case – compared to the $E_r = 0$ case. The shift is more pronounced for low-energy particles, as their motion is more sensitive to changes in E_r. The particle in Figure 6 is of this type.

The second major loss mechanism involves barely trapped particles. In Case +, the positive E_r pushes barely trapped particles into helically trapped orbits, which are generally better confined than barely trapped particles, and are even more so when under a positive E_r. Conversely, in Case –, the negative E_r pushes some particles into barely trapped orbits, which are poorly confined. A particle of this type is shown in

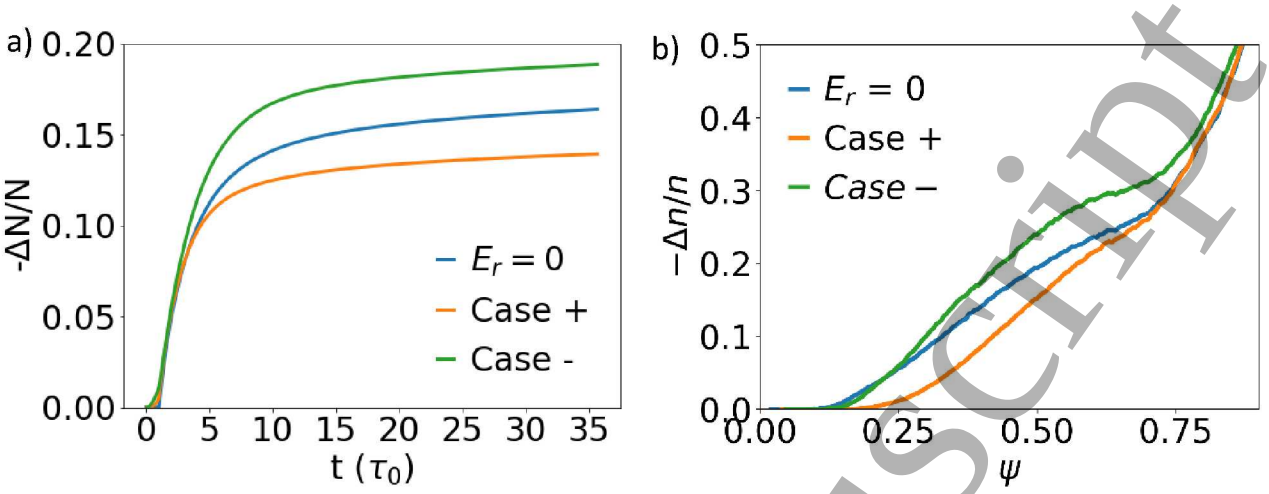

Figure 10 a) Fraction of lost particles as a function of time. Particles lost on first orbit in the $E_r = 0$ case are removed from simulation b) fraction of lost particles at the end of simulation as a function of initial position

Figure 7 which displays the trajectory of a particle in a barely trapped orbit under the effects of the 3 experimentally informed E_r profiles. As shown in Figure 7b, the particle in Case – is pushed into a banana like orbit. By examining Figure 7a, we see that this particle then drifts slightly further out after each banana bounce. It eventually reaches a flux surface of large enough B field variation to force the particle into a helically trapped orbit until it drifts out past the separatrix. This effect is shown as well in Figure 8, where particles with λ values between 0.8 and 1 are lost more frequently in Case – and less frequently in Case +.

Figure 9 shows the fraction of particles lost from locations on a flux surface. The particles lost due to the negative E_r can be seen in the Case – column of Figure 9. The region in real space from which these particles are lost forms a volume around the plasma, which we may be able to target with NBI to influence E_r. This volume is centered around the surface formed approximately by the B = $0.7B_0$ surface but stretches towards the high B field regions with two arms reached by the bounce motion of these lost particles. This volume can be viewed as both the volume in real space from which trapped particles are lost as well as the volume swept by trapped particles on the boundary to barely trapped as they move through the plasma. The existence of this volume provides evidence that we can use targeted perpendicular NBI to control E_r by injecting into regions that will quickly exit the plasma.

The radial electric field has a significant impact on the overall confinement of energetic particles. Figure 10 shows the fraction of particles lost vs time as well as the fraction lost at the end of simulation as a function of radius where $N = \int_0^{\psi_w} n\, d\psi$. As shown in Figure 10, imposing a positive E_r improves confinement, whereas setting a negative E_r at the plasma edge degrades confinement. Examining Figure 5b, we observe that while E_r in Case + and Case – diverge at around $\psi = 0.25$, E_r in Case – only becomes negative around $\psi = 0.6$. However, as shown in Figure 10b, more particles in Case – are lost from regions much deeper towards the core compared to the No E_r case. These particles are helically trapped or boundary particles that reach the negative E_r region as they drift towards the inside of the torus, then experience increased radial drift and are lost to the separatix. These results are consistent with our analysis of the effects of constant E_r presented in section 3 as the positive E_r closer to the core shifts particles into hellically trapped orbits while the negative E_r on the outer edge of Case – takes these particles, and increases their radial drift, letting them reach the last closed flux surface.

5. Conclusions

We have analyzed the effects of the radial electric field in the electron root on the collisionless loss of EPs in LHD. E_r regardless of sign has very little impact on passing particles, which are generally well confined.

A positive E_r reinforces the poloidal precession of particles, while negative E_r reduces this precession rate. As trapped particles precess poloidally, they drift radially due to the B(1,0) toroidicity. This radial drift

direction does not depend on precession rate, but on position, so a slower precession rate allows particles to spend more time in one location drifting in one direction radially. In this way, a poitive E_r reduces while a negative E_r increases radial drift of trapped particles in LHD.

Barely trapped particles are poorly confined as their orbits are not periodic. E_r affectes their radial drift in the same way that it effects helically trapped particles. A positive E_r can push barely trapped orbits towards helically trapped orbits, which are better confined. A negative E_r does the opposite, pushing trapped orbits to barely trapped orbits, further degrading confinement.

The vast majority of lost particles in LHD come from trapped or barely trapped particle orbits. These losses are reduced under positive E_r, and exacerbated under negative E_r and Case -. While E_r does have a stronger effect on lower energy trapped ions, E_r is shown to have a noticeable effect on the confinement of trapped ions at energies at least 12 times greater than the variation in potential. Analysis of the effects of E_r on the distribution of lost particles agrees with our analysis of its effects on particle orbits.

While this paper discusses neoclassical collisionless transport, the effects of E_r on collisional diffusion are discussed in [3], [14], [15], where it is shown that confinement will be further improved in the electron root. This work will be continued in a study of experiments and self consistent simulations of E_r in LHD including the effects of realistic 5D EP distributions produced through NBI. The end goal is to provide further insight into the control of E_r through NBI and ECRH to improve confinement.

Acknowledgements

We would like to thank William Heidbrink, Hongxuan Zhu, Elizabeth Paul, Handi Huang, and Wenhao Wang for many helpful discussions. This work has been partially supported by grants from the DOE SciDAC Hifistell and INCITE projects. This work used computing resources at NERSC and ORNL.

Data Availability

The data supporting the findings of this study are available in the LHD experiment data repository at https://doi.org/10.57451/lhd.analyzed-data.

References

[1] L. Spitzer Jr., "The Stellarator Concept," *Phys. Fluids*, vol. 1, no. 4, pp. 253–264, Jul. 1958, doi: 10.1063/1.1705883.

[2] A. H. Boozer, "Stellarators as a fast path to fusion," *Nucl. Fusion*, vol. 61, no. 9, p. 096024, Aug. 2021, doi: 10.1088/1741-4326/ac170f.

[3] A. A. Galeev, R. Z. Sagdeev, H. P. Furth, and M. N. Rosenbluth, "Plasma Diffusion in a Toroidal Stellarator," *Phys. Rev. Lett.*, vol. 22, no. 11, pp. 511–514, Mar. 1969, doi: 10.1103/PhysRevLett.22.511.

[4] H. Nuga *et al.*, "Degradation of fast-ion confinement depending on the neutral beam power in MHD quiescent LHD plasmas," *Nucl. Fusion*, vol. 64, no. 6, p. 066001, Apr. 2024, doi: 10.1088/1741-4326/ad3971.

[5] E. J. Paul, A. Bhattacharjee, M. Landreman, D. Alex, J. L. Velasco, and R. Nies, "Energetic particle loss mechanisms in reactor-scale equilibria close to quasisymmetry," *Nucl. Fusion*, vol. 62, no. 12, p. 126054, Nov. 2022, doi: 10.1088/1741-4326/ac9b07.

[6] P. J. Bonofiglo, D. W. Dudt, and C. P. S. Swanson, "Fast ion confinement in quasi-axisymmetric stellarator equilibria," *Nucl. Fusion*, vol. 65, no. 2, p. 026050, Jan. 2025, doi: 10.1088/1741-4326/ada56d.

[7] H. Biglari, P. H. Diamond, and P. W. Terry, "Influence of sheared poloidal rotation on edge turbulence," *Phys. Fluids B Plasma Phys.*, vol. 2, no. 1, pp. 1–4, Jan. 1990, doi: 10.1063/1.859529.

[8] Z. Lin, T. S. Hahm, W. W. Lee, W. M. Tang, and R. B. White, "Turbulent Transport Reduction by Zonal Flows: Massively Parallel Simulations," *Science*, vol. 281, no. 5384, pp. 1835–1837, Sep. 1998, doi: 10.1126/science.281.5384.1835.

[9] K. Hanatani and F.-P. Penningsfeld, "Resonant superbanana and resonant banana losses of injected fast ions in Heliotron E and Wendelstein VII-A: effects of the radial electric field," *Nucl. Fusion*, vol. 32, no. 10, p. 1769, Oct. 1992, doi: 10.1088/0029-5515/32/10/I06.

[10] K. Ida *et al.*, "Control of the radial electric field shear by modification of the magnetic field configuration in LHD," *Nucl. Fusion*, vol. 45, no. 5, p. 391, Apr. 2005, doi: 10.1088/0029-5515/45/5/010.

[11] P. Helander, A. G. Goodman, C. D. Beidler, M. Kuczyński, and H. M. Smith, "Optimised stellarators with a positive radial electric field," May 29, 2024, *arXiv*: arXiv:2405.07085. doi: 10.48550/arXiv.2405.07085.

[12] K. Ida, "Experimental studies of the physical mechanism determining the radial electric field and its radial structure in a toroidal plasma," *Plasma Phys. Control. Fusion*, vol. 40, no. 8, p. 1429, Aug. 1998, doi: 10.1088/0741-3335/40/8/002.

[13] M. Landreman and P. J. Catto, "Effects of the radial electric field in a quasisymmetric stellarator," *Plasma Phys. Control. Fusion*, vol. 53, no. 1, p. 015004, Nov. 2010, doi: 10.1088/0741-3335/53/1/015004.

[14] H. E. Mynick, "Effect of collisionless detrapping on nonaxisymmetric transport in a stellarator with radial electric field," *Phys. Fluids*, vol. 26, no. 9, pp. 2609–2615, Sep. 1983, doi: 10.1063/1.864452.

[15] H. E. Mynick and W. N. G. Hitchon, "Effect of the ambipolar potential on stellarator confinement," *Nucl. Fusion*, vol. 23, no. 8, p. 1053, Aug. 1983, doi: 10.1088/0029-5515/23/8/006.

[16] X. D. Du *et al.*, "Resistive Interchange Modes Destabilized by Helically Trapped Energetic Ions in a Helical Plasma," *Phys. Rev. Lett.*, vol. 114, no. 15, p. 155003, Apr. 2015, doi: 10.1103/PhysRevLett.114.155003.

[17] M. Nishiura *et al.*, "Core density profile control by energetic ion anisotropy in LHD," *Phys. Plasmas*, vol. 31, no. 6, p. 062505, Jun. 2024, doi: 10.1063/5.0201440.
[18] K. Ida *et al.*, "Reduction of Ion Thermal Diffusivity Associated with the Transition of the Radial Electric Field in Neutral-Beam-Heated Plasmas in the Large Helical Device," *Phys. Rev. Lett.*, vol. 86, no. 23, pp. 5297–5300, Jun. 2001, doi: 10.1103/PhysRevLett.86.5297.
[19] T. Watanabe *et al.*, "Magnetic field structure and confinement of energetic particles in the LHD," *Nucl. Fusion*, vol. 46, no. 2, p. 291, Jan. 2006, doi: 10.1088/0029-5515/46/2/013.
[20] J. Y. Fu, J. H. Nicolau, P. F. Liu, X. S. Wei, Y. Xiao, and Z. Lin, "Global gyrokinetic simulation of neoclassical ambipolar electric field and its effects on microturbulence in W7-X stellarator," *Phys. Plasmas*, vol. 28, no. 6, p. 062309, Jun. 2021, doi: 10.1063/5.0047291.
[21] V. V. Nemov, S. V. Kasilov, W. Kernbichler, and G. O. Leitold, "Poloidal motion of trapped particle orbits in real-space coordinates," *Phys. Plasmas*, vol. 15, no. 5, p. 052501, May 2008, doi: 10.1063/1.2912456.
[22] A. LeViness *et al.*, "Energetic particle optimization of quasi-axisymmetric stellarator equilibria," *Nucl. Fusion*, vol. 63, no. 1, p. 016018, Dec. 2022, doi: 10.1088/1741-4326/aca4e3.
[23] P. Helander and A. N. Simakov, "Intrinsic Ambipolarity and Rotation in Stellarators," *Phys. Rev. Lett.*, vol. 101, no. 14, p. 145003, Sep. 2008, doi: 10.1103/PhysRevLett.101.145003.
[24] X. Xu *et al.*, "Active generation and control of radial electric field by local neutral beamlets injection in tokamaks," *Nucl. Fusion*, vol. 64, no. 2, p. 026012, Jan. 2024, doi: 10.1088/1741-4326/ad169e.
[25] Y.-S. Na, T. S. Hahm, P. H. Diamond, A. Di Siena, J. Garcia, and Z. Lin, "How fast ions mitigate turbulence and enhance confinement in tokamak fusion plasmas," *Nat. Rev. Phys.*, vol. 7, no. 4, pp. 1–13, Apr. 2025, doi: 10.1038/s42254-025-00814-8.
[26] A. Iiyoshi *et al.*, "Overview of the Large Helical Device project," *Nucl. Fusion*, vol. 39, no. 9Y, p. 1245, Sep. 1999, doi: 10.1088/0029-5515/39/9Y/313.
[27] T. Ido *et al.*, "6 MeV heavy ion beam probe on the Large Helical Device," *Rev. Sci. Instrum.*, vol. 77, no. 10, p. 10F523, Oct. 2006, doi: 10.1063/1.2338311.
[28] M. Nishiura *et al.*, "Enhanced beam transport via space charge mitigation in a multistage accelerator for fusion plasma diagnostics," Jul. 28, 2025, *arXiv*: arXiv:2507.20948. doi: 10.48550/arXiv.2507.20948.
[29] C. Suzuki, K. Ida, Y. Suzuki, M. Yoshida, M. Emoto, and M. Yokoyama, "Development and application of real-time magnetic coordinate mapping system in the Large Helical Device," *Plasma Phys. Control. Fusion*, vol. 55, no. 1, p. 014016, Dec. 2012, doi: 10.1088/0741-3335/55/1/014016.
[30] S. P. Hirshman and J. C. Whitson, "Steepest-descent moment method for three-dimensional magnetohydrodynamic equilibria," *Phys. Fluids*, vol. 26, no. 12, pp. 3553–3568, Dec. 1983, doi: 10.1063/1.864116.
[31] R. Sanchez, S. P. Hirshman, A. S. Ware, L. A. Berry, and D. A. Spong, "Ballooning stability optimization of low-aspect-ratio stellarators*," *Plasma Phys. Control. Fusion*, vol. 42, no. 6, p. 641, Jun. 2000, doi: 10.1088/0741-3335/42/6/303.
[32] P. Liu *et al.*, "Regulation of Alfvén Eigenmodes by Microturbulence in Fusion Plasmas," *Phys. Rev. Lett.*, vol. 128, no. 18, p. 185001, May 2022, doi: 10.1103/PhysRevLett.128.185001.
[33] J. W. Connor and R. J. Hastie, "Neoclassical diffusion in an l = 3 stellarator," *Phys. Fluids*, vol. 17, no. 1, pp. 114–123, Jan. 1974, doi: 10.1063/1.1694573.
[34] B. B. Kadomtsev and O. P. Pogutse, "Trapped particles in toroidal magnetic systems," *Nucl. Fusion*, vol. 11, no. 1, p. 67, Jan. 1971, doi: 10.1088/0029-5515/11/1/010.
[35] T. Watanabe *et al.*, "Magnetic field structure and confinement of energetic particles in the LHD," *Nucl. Fusion*, vol. 46, no. 2, p. 291, Jan. 2006, doi: 10.1088/0029-5515/46/2/013.